

A dual-band flexible frequency selective surface with miniaturized elements and maximally flat (Butterworth) response

This content has been downloaded from IOPscience. Please scroll down to see the full text.

2014 Chinese Phys. B 23 047303

(<http://iopscience.iop.org/1674-1056/23/4/047303>)

View [the table of contents for this issue](#), or go to the [journal homepage](#) for more

Download details:

IP Address: 159.226.165.21

This content was downloaded on 25/03/2015 at 07:25

Please note that [terms and conditions apply](#).

A dual-band flexible frequency selective surface with miniaturized elements and maximally flat (Butterworth) response*

Wang Xiu-Zhi(王秀芝)^{a)b)}, Gao Jin-Song (高劲松)^{a)}, Xu Nian-Xi(徐念喜)^{a)†}, and Liu Hai(刘 海)^{a)}

^{a)}Key Laboratory of Optical System Advanced Manufacturing Technology, Changchun Institute of Optics, Fine Mechanics and Physics, Chinese Academy of Sciences, Changchun 130033, China

^{b)}University of Chinese Academy of Sciences, Beijing 100049, China

(Received 2 July 2013; revised manuscript received 28 September 2013; published online 10 February 2014)

A dual-band flexible frequency selective surface (FSS) with miniaturized elements and maximally flat (Butterworth) response is presented in this paper. It is composed of three metallic layers, which are fabricated on thin flexible polyimide substrates and bonded together using thin bonding films. The overall thickness of the proposed structure is only about 0.3 mm, making it an attractive choice for conformal FSS applications. All the three layers can constitute a miniaturized-element FSS (MEFSS) and produce the first pass-band with miniaturization property, while the up and bottom layers can constitute a symmetric biplanar FSS and produce the second pass-band with maximally flat (Butterworth) response. The two pass-bands are independent and there is a wide band spacing up to 30 GHz between them. The principles of operation, the simulated results by using the vector modal matching method, and the experimental values of the fabricated prototype are also presented and discussed.

Keywords: bandpass filters, flexible structures, frequency selective surfaces

PACS: 73.61.-r, 73.90.+f

DOI: 10.1088/1674-1056/23/4/047303

1. Introduction

Frequency selective surfaces (FSSs) have been the subject of intensive investigation for many years. An FSS is a one-dimensional (1D) or two-dimensional (2D) periodic array of patch or aperture elements on a dielectric layer. It acts as a spatial filter with band stop or band pass capability depending on the element type (i.e., aperture or patch). Owing to their superior frequency selective properties, FSSs have been widely used in antenna design, surface wave manipulation, and radar cross section (RCS) management.^[1-4]

With the advent of multifunctional systems, the need for complex FSSs with favorable properties, such as miniaturized elements, multi-bands, maximally flat (Butterworth) response, etc., is on the rise. Therefore, many techniques for designing FSS have been presented. In Ref. [5], a miniaturized-element FSS (MEFSS) that is based on coupling mechanism was proposed. It is made up of a capacitive patches array printed on one side of a dielectric substrate and an inductive wire mesh printed on the other side. Thereafter, the MEFSSs have been extensively studied by many researchers.^[6-11] The approach to the design of MEFSSs in Ref. [5] can remarkably reduce the size of the unit cells and improve the stability of the incidence angle. However, it increases not only the thickness of the structure, but also the insertion loss of the FSS. It restricts the applications where low-profile and conformal FSSs are required. To achieve a multi-frequency response, the FSSs with combination or fractal elements are generally

exploited.^[12-14] However, there are large-incidence angle and wide band spacing limits for those structures, above which their high order resonances will deteriorate due to the interaction between the current modes of the elements. In addition, the modified version of MEFSSs also has multi-bands (dual-band) that are created by embedding resonant elements in the capacitive patches, as presented in Ref. [15]. The two pass-bands are independent and based on coupling and resonance mechanisms, respectively. To obtain maximally flat (Butterworth) response, the symmetric biplanar FSSs, obtained by mounting two identical layers behind each other, have been discussed in Chapter 7 of Ref. [1]. In such a case, only at a crucial coupling can the system have a maximally flat (Butterworth) response with a broad flat top and sharp cut off.

In this paper, we make further modification to the MEFSSs. We design a structure with three metallic layers: an inductive wire mesh in the middle side and two capacitive layers with square patches at outsides, and choose square loop slots as resonators embedded in capacitive square patches. All of the layers are fabricated on thin flexible polyimide substrates and bonded together using thin bonding films. The overall thickness of the proposed structure is only about 0.3 mm, making it an attractive choice for conformal FSS applications. In a way similar to that discussed in Ref. [15], the structure also has two independent pass-bands based on different mechanisms. Moreover, there is a wide band spacing (about 30 GHz) between the pass-bands for the highly selected elements type

*Project supported by the Third Innovation Fund of Changchun Institute of Optics and Fine Mechanics and Physics (Grant No. 093Y32J090).

†Corresponding author. E-mail: xnxlzhy999@126.com

and dielectric parameters. Paying attention to the square loop slots, it can be observed that they can constitute a symmetric biplanar system. By properly choosing the parameters of the thin flexible substrates and the bonding films, the symmetric biplanar system will be at a crucial coupling and the second pass-band will have a maximally flat (Butterworth) response. So, in this paper, we can obtain two pass-bands with miniaturization property and maximally flat (Butterworth) response, respectively. The first pass-band is in Ku-band with a central frequency of 13 GHz and -3 -dB bandwidth of 3.7 GHz, the second pass-band has a property of maximally flat (Butterworth) response with a flat top from 42.6 GHz to 49.6 GHz, and the -3 -dB bandwidth of the second pass-band is up to 15.3 GHz.

In this paper, the structure will be analyzed by using the equivalent circuit model in Section 2, and the simulated results will be presented and discussed in Section 3. In Section 4, the prototype fabricated by using the standard lithography and the experimental results measured in free-space environment are also presented to verify the design and simulations. Finally, the conclusion of the work is drawn in Section 5.

2. Principles of operation

The proposed FSS is constituted by cascading three metal layers, as shown in Fig. 1. The middle layer consists of a 2D periodic array of metal strips in the form of a wire grid. As such, it acts as an inductive surface. The top and bottom metal layers consist of 2D periodic arrays of patches, and each patch is embedded in a square loop slot. The two layers correspond to capacitances in a circuit model, since they act as capacitive surfaces. Furthermore, they can also work as resonance surfaces due to the appearances of the square loop slots. By combining the three layers, the first pass-band with miniaturization property can be achieved by coupling the electric and magnetic field of the incident wave. Meanwhile, the two resonance surfaces with square loop slots constitute a symmetric biplanar FSS and result in the second pass-band. The two pass-bands are independent because they originate from different mechanisms, which will save trouble in the multi-band FSS using combined elements or fractal elements. To meet the conditions of critical coupling, a polyimide is selected as a flexible substrate material with thickness $d_1 = 0.0254$ mm, dielectric constant $\epsilon_{r1} = 3.0$, and a loss tangent $\tan\delta_1 = 0.005$, while the bonding film is selected to have $d_2 = 0.1$ mm, $\epsilon_{r2} = 2.6$, and $\tan\delta_2 = 0.0035$. Then, the second pass-band has a property of maximally flat (Butterworth) response with a broad flat top and sharp cut off. Furthermore, the flexible structure has an extremely low profile and an overall thickness of about 0.3 mm, making it an attractive choice for conformal FSS applications.

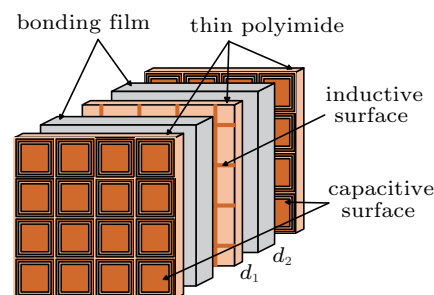


Fig. 1. (color online) Structural diagram of the FSS.

Figure 2(a) shows the elements and equivalent circuit models of inductive and capacitive surfaces. The dimensions given in it are $D_x = D_y = 2.4$ mm, $W_1 = 0.15$ mm, $D_1 = 2.25$ mm, $D_2 = 1.95$ mm, and $D_3 = 1.65$ mm. When the FSS is exposed to the normal incidence, the unit cell of inductive surface can be equal to an inductor (L_1). While the unit cell of capacitive surface can be equal to a parallel LC circuit (L_2 and C_2) in series with a capacitor C_1 (the patch outside the square loop slot represents inductance L_2 , and the gaps g_1 and g_2 represent capacitors C_1 and C_2 , respectively). The equivalent circuit of the FSS can, therefore, be shown as in Fig. 2(b). In the circuit, $Z_0 = 377 \Omega$ is the free space impedance; Z_1 and Z_2 are the intrinsic impedances of the polyimide substrate and the thin bonding film, respectively; $Z_1 = Z_0/(\epsilon_{r1})^{1/2}$; $Z_2 = Z_0/(\epsilon_{r2})^{1/2}$; K_1 and K_2 are the magnetic coupling coefficients between L_1 and L_2 that represent the magnetic interactions between the adjacent metallic layers.

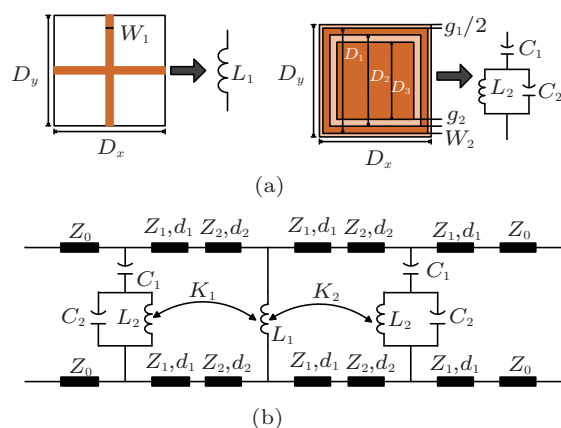


Fig. 2. (color online) (a) Elements and equivalent circuit models of inductive and capacitive surfaces, and (b) the equivalent circuit model of the FSS.

In Fig. 2(b), the L_2 - C_2 connected in parallel mainly determines the frequency of the second pass band. However, the central frequency of the first pass-band is mainly determined by the values of C_1 , L_1 , and the thickness values of the dielectrics d_1 and d_2 .

3. Results and discussion

In order to exactly calculate the transmittance of this structure, the vector modal matching method is introduced, which is one of the stable convergent full-wave numerical analysis methods.^[16,17] The influences of the scan angles and structure parameters on the frequency response are also revealed in the following.

Figure 3 shows the transmission coefficient of the FSS at normal incidence. There are two pass-bands with a wide band spacing of about 30 GHz. The first one is in Ku-band with a central frequency of 13 GHz and -3 -dB bandwidth of 3.7 GHz. The second one has a property of maximally flat (Butterworth) response with flat top and sharp cut off. In the flat top there is a very small valley with a depth of -0.828 -dB at 47.4 GHz between two peaks at 42.6 GHz and 49.6 GHz. This happens because that the parameters of the structure do not meet the conditions of critical coupling very well. The -3 -dB bandwidth of the second pass-band is 15.3 GHz. The period size of this FSS is only about $0.104\lambda_1$, where λ_1 is the wavelength at the central frequency of the first pass-band. In conclusion, the proposed FSS can obtain two independent and greatly separated pass-bands with miniaturization property and maximally flat (Butterworth) response, respectively.

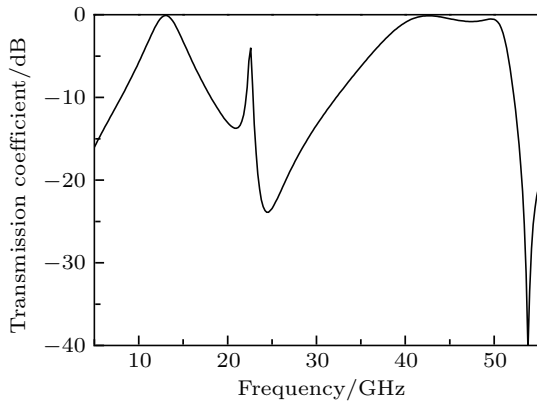


Fig. 3. Frequency response of the FSS at normal incidence.

In Fig. 3, there is a spurious resonance at 22 GHz between the two pass bands. This is mainly caused by the interaction between the patches outside the square loop slot of the capacitive surfaces, which represents inductance L_2 in a circuit model. In fact, for many practical applications it is so narrow that it is of minor consequence.

Figure 4 shows the transmission coefficients of the FSS at oblique incident angles (maximal incident angle is 60° with respect to normal direction) for TE and TM polarizations.

It is observed that with the increase of the incident angle, the central frequency of the first pass-band only increases 1.2 GHz and 1 GHz for TE and TM polarizations, respectively. While the -3 -dB bandwidth of the first pass-band reduces from 3.7 GHz to 2.1 GHz for TE polarization, but increases

from 3.7 GHz to 7.1 GHz for TM polarization. It has less sensitivity to the incident angle and polarization.

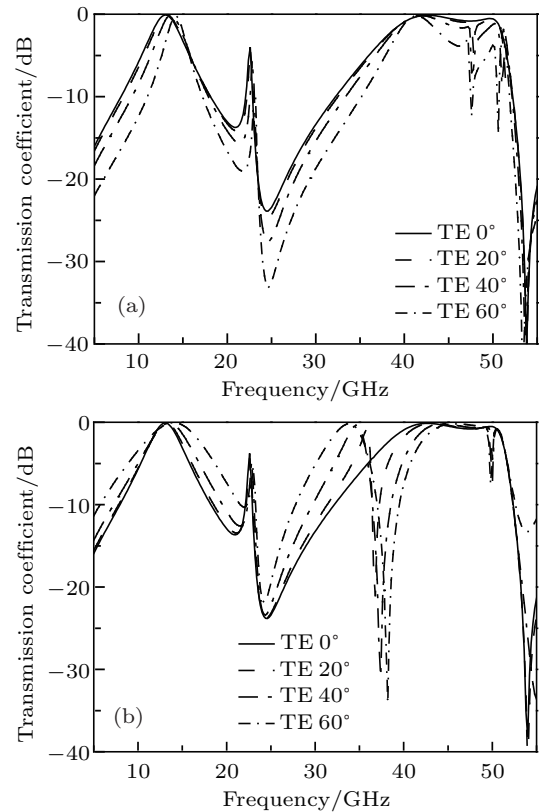


Fig. 4. Frequency responses of FSS at different incident angles for (a) TE polarization and (b) TM polarization.

For the second pass-band, as observed in Fig. 4(a) for TE polarization, the depth of the valley increases as scan angle increases from 0° to 60° , the first peak always stays at about 41 GHz with a transmission coefficient higher than -0.5 -dB and the -3 -dB bandwidth wider than 6 GHz, while the second peak remains well until the incident angle is over 40° . For the TM polarization in Fig. 4(b), the modal interaction nulls occur around 37 GHz, but a good pass-band with flat top and sharp cut off remains at frequencies over 40 GHz. As the scan angle increases from 0° to 60° , the depth of the valley becomes smaller. Between 43 GHz and 49 GHz, the frequency response keeps well with transmission coefficient higher than -1 -dB and the -3 -dB bandwidth wider than 8 GHz. In conclusion, the structure has an excellent high order pass band.

Figure 5 shows the influences of the width of the grad W_1 in the inductive surface on the transmission coefficient of the FSS at normal incidence. When W_1 increases from 0.075 mm to 0.3 mm, the central frequency of the first pass-band shifts from 12 GHz to 14.2 GHz and the -3 -dB bandwidth of the first pass-band decreases from 4.7 GHz to 2.8 GHz. For the second pass-band, with the increase of W_1 , the first peak shifts toward high frequency while the second peak remains unchanged, and the -3 -dB bandwidth of the second pass-band decreases from 15.8 GHz to 9.6 GHz. In addition, the depth

of the valley between the two peaks gradually decreases and the flat top becomes more visible. From the above discussion, it can be obtained that the inductive surface has an influence not only on the first pass-band based on the coupling mechanism, but also on the second one that is based on the resonance mechanism.

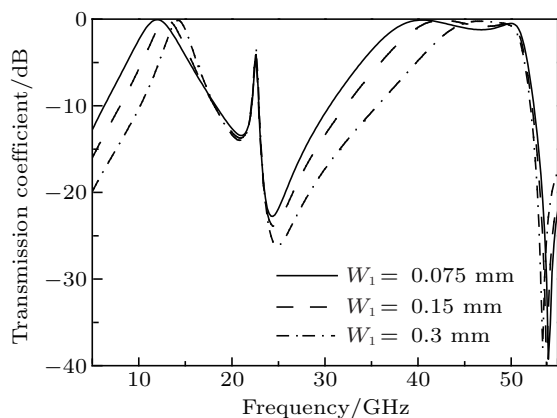


Fig. 5. Influences of W_1 on transmission characteristic at normal incidence.

Figure 6 shows the influences of the size D_1 of the square patch in the capacitive surface on the transmission coefficient of the FSS at normal incidence. When D_1 increases from 2.175 mm to 2.325 mm, the central frequency of the first pass-band shifts from 14.6 GHz to 11.2 GHz, and the -3 -dB bandwidth of the first pass-band decreases from 4.6 GHz to 2.8 GHz, while the second pass-band remains unchanged.

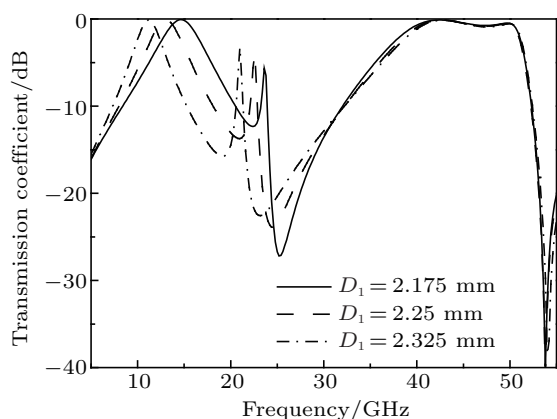


Fig. 6. Influences of D_1 on transmission characteristic at normal incidence.

We then analyze the influences of D_2 and D_3 (by keeping the width of the square loop slot $g_2 = (D_2 - D_3)/2 = 0.15$ mm unchanged) on the transmission of the FSS at normal incidence. Figure 7 shows the transmission coefficients of the FSS for $(D_2 = 1.875$ mm, $D_3 = 1.575$ mm), $(D_2 = 1.95$ mm, $D_3 = 1.65$ mm), and $(D_2 = 2.025$ mm, $D_3 = 1.725$ mm), respectively. It is observed that, with the increase of the length of the side for the slot, the first pass-band keeps unchanged,

while the second pass-band shifts toward low frequencies with the width of the flat top and the -3 -dB bandwidth remaining constant.

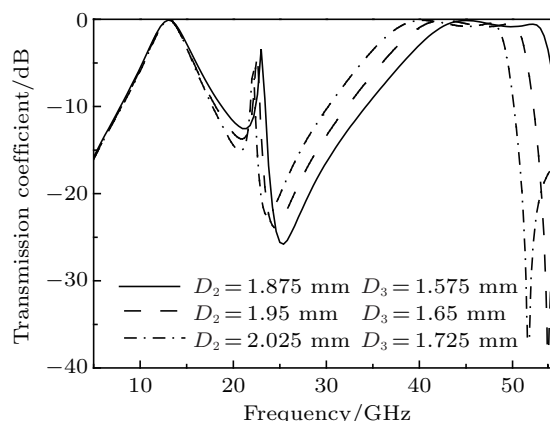


Fig. 7. Influences of D_2 and D_3 on transmission characteristic at normal incidence.

From these results in Figs. 6 and 7, we can obtain that the sizes of square patches in the capacitive surfaces mainly influence the first pass-band, while the lengths of the square loop slots embedded in the patches mainly influence the second pass-band. This demonstrates that the first pass-band is based on the coupling mechanism while the second one is based on the resonance mechanism. These achievements further confirm that the two pass-bands are independent and can be tuned respectively by changing the dimensions of the structure.

4. Experimental verification

In order to experimentally verify the accuracy of the analysis and simulations, the structure shown in Fig. 1 was fabricated. As shown in Fig. 8, the dimension of the sample is 400 mm \times 400 mm. The capacitive and inductive surfaces of the structure were fabricated through a standard etching of copper on 0.0254-mm-thick flexible polyimide substrates. Then, the three metal layers on polyimide substrates were bonded together by two aerial bonding films ($\epsilon_{r2} = 2.6$ and $\tan \delta_2 = 0.0035$) with precise alignment.



Fig. 8. (color online) The FSS fabricated using standard lithography.

The measurement of the second pass-band requires higher machining precision and alignment precision of the three metal layers, and it should be operated in a waveguide environment. So, we only measured the first pass-band in a free-space environment using an Agilent N5244A vector network analyzer. The measurement system in free-space environment is shown in Fig. 9. Besides the vector network analyzer, the measurement comprises a pair of lens antenna, a bearing bracket, and a rotatable table.

Figure 10 shows a comparison between the measured and simulated results for TE polarization. It can be seen that they are in good agreement in a range from 0° to 60° . This experi-

mentally verifies the accuracy of the numerical analysis.

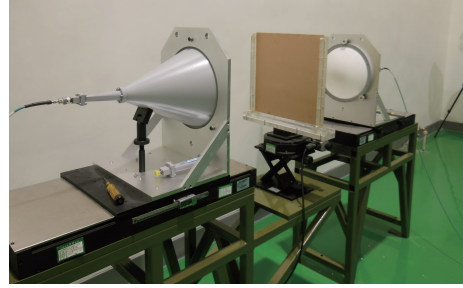


Fig. 9. (color online) Free-space measurement system.

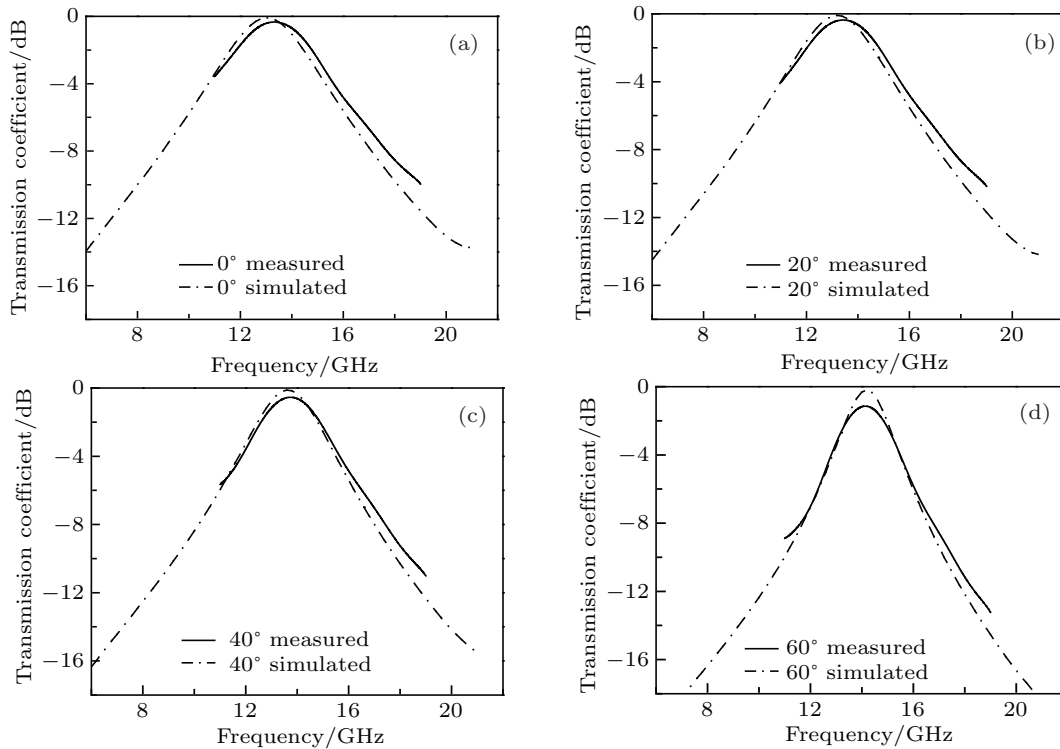


Fig. 10. Comparisons between measured and simulated results of the first pass-band at incident angles of (a) 0° , (b) 20° , (c) 40° , and (d) 60° .

5. Conclusions

In this paper, a dual-band flexible FSS with miniaturized elements and maximally flat (Butterworth) response is presented. The equivalent circuit model of the FSS is used for performance analysis, and the structure is simulated by the vector modal matching method. It is demonstrated that the first pass-band with miniaturization property is produced by the direct near-field coupling between the three layers, while the second pass-band with maximally flat (Butterworth) response is produced by the resonance of the square loop slots embedded in the patches of the capacitive surfaces. The first pass-band is in Ku-band with a central frequency of 13 GHz and the period size of this FSS is only about $0.104 \lambda_1$. The second pass-band has a property of maximally flat (Butterworth) response with flat top and sharp cut off. In the flat top there is a very small

valley with a depth of -0.828 dB at 47.4 GHz between two peaks at 42.6 GHz and 49.6 GHz. The -3 -dB bandwidths of the two pass-bands are about 3.7 GHz and 15.3 GHz. Unlike the conventional multi-band FSSs with combined or fractal elements, the two pass-bands of the modified MEFSS are independent and have wide band spacing (about 30 GHz). In particular, the second one is more attractive. Furthermore, the flexible structure has an extremely low profile and an overall thickness of about 0.3 mm. Finally, the measurement results for the fabricated prototype using lithography are in good agreement with the simulated values, which experimentally verifies the accuracy of the numerical analysis. The proposed structure can be useful for designing dual-band flexible FSS with a small overall profile, wide band spacing, and especially with an excellent high order pass band.

References

- [1] Munk B A 2000 *Frequency Selective Surfaces: Theory and Design* (New York: Wiley)
- [2] Jia H Y, Gao J S and Feng X G 2009 *Chin. Phys. B* **18** 1227
- [3] Wang S S, Gao J S, Liang F C, Wang Y S and Chen X 2011 *Acta Phys. Sin.* **60** 050703 (in Chinese)
- [4] Zhang J, Gao J S and Xu N X 2013 *Acta Phys. Sin.* **62** 147304 (in Chinese)
- [5] Sarabandi K and Behdad N 2007 *IEEE Trans. Antennas Propag.* **55** 1239
- [6] Bayatpur F and Sarabandi K 2008 *IEEE Trans. Microw. Theory Tech.* **56** 774
- [7] Al-Joumayly M and Behdad N 2009 *IEEE Trans. Antennas Propag.* **57** 452
- [8] Behdad N, Al-Joumayly M and Salehi M 2009 *IEEE Trans. Antennas Propag.* **57** 460
- [9] Bayatpur F and Sarabandi K 2010 *IEEE Trans. Antennas Propag.* **58** 1214
- [10] Xu N X, Feng X G, Wang Y S, Chen X and Gao J S 2011 *Acta Phys. Sin.* **60** 114102 (in Chinese)
- [11] Moallem M and Sarabandi K 2012 *IEEE Transactions on Terahertz Science and Technology* **2** 333
- [12] Romeu J and Rahmat-Samii Y 2000 *IEEE Trans. Antennas Propag.* **48** 1097
- [13] Gianvittorio J P, Rahmat-Samii Y and Romeu J 2001 *IEEE AP-S Int. Symp. Dig.* 640
- [14] Wang X Z, Gao J S and Xu N X 2013 *Acta Phys. Sin.* **62** 167307 (in Chinese)
- [15] Salehi M and Behdad N 2008 *IEEE Microwave and Wireless Propagation Letters* **18** 785
- [16] Chen C C 1970 *IEEE Trans. Antennas Propag.* **AP-18** 660
- [17] Mittra R, Chan C H and Cwik T 1988 *Proc. IEEE* **76** 1593